Journal of Archaeological Science 121 (2020) 105198

Contents lists available at ScienceDirect

Journal of Archaeological Science

journal homepage: http://www.elsevier.com/locate/jas

Implications for paleomobility studies of the effects of quaternary volcanism on bioavailable strontium: A test case in North Patagonia (Argentina)

Alejandro Serna [a,*], Luciano Prates [a], Emiliano Mange [a], Domingo C. Salazar-García [b,c,d], Clement P. Bataille [e,**]

[a] CONICET-División Arqueología, Facultad de Ciencias Naturales y Museo, Universidad Nacional de La Plata, Anexo Museo, Av. 122 y 60 (1900), La Plata, Argentina
[b] Grupo de Investigación en Prehistoria IT-1223-19 (UPV-EHU)/IKERBASQUE-Basque Foundation for Science, Vitoria, Spain
[c] Department of Geological Sciences, University of Cape Town, Cape Town, South Africa
[d] Departament de Prehistòria, Arqueologia i Història Antiga, Universitat de València, València, Spain
[e] Department of Earth and Environmental Sciences, University of Ottawa, 120 University, Ottawa, ON, K1N 6N5, Canada

ARTICLE INFO

Keywords:
Patagonia
Archaeology
Provenance
Bioavailable strontium
Isoscape
Volcanic sediment
Atmospheric deposition

ABSTRACT

Strontium isotopes ($^{87}Sr/^{86}Sr$) are used as geochemical tracers for paleomobility studies because they display predictable and stable patterns in ecosystems primarily controlled by the underlying geological regimes. While bedrock geology is stable over thousands of years, geomorphological processes can influence the $^{87}Sr/^{86}Sr$ in ecosystems over archeologically relevant timescales. Among these geomorphological processes, the deposition and reworking of volcanic sediments over Quaternary timescales are little studied but could be an important control of $^{87}Sr/^{86}Sr$ variations in many archeological regions. North Patagonia is a key archeological region to address animal and human movements, and an ideal location to test the influence of Quaternary volcanism on $^{87}Sr/^{86}Sr$ variation as it is located downwind of major volcanic centers. In this study, we aim to assess the main environmental and geological controls of bioavailable $^{87}Sr/^{86}Sr$ and to build a high-resolution isoscape using a machine learning regression framework for forthcoming paleomobility studies. We sampled several locations and analyzed different types of samples ($N = 94$). The ratios show a limited range of variation, which is not related to the bedrock geology. Rather, bioavailable $^{87}Sr/^{86}Sr$ variations display a progressive increase going eastward (away from the Andes), following dust aerosol deposition and elevation variations ($R^2 = 0.71$, RMSE = 0.00041). We argue that this trend relates to the deposition and reworking of unradiogenic volcanic sediments by aeolian, fluvial and glacial erosion during the Quaternary. As most of this sediment reworking occurred during glacial periods, the current bioavailable $^{87}Sr/^{86}Sr$ variations across the study area likely represent a long-term average that varied little during the Holocene. Consequently, our isoscape provides a solid base for Holocene paleomobility studies in North Patagonia and underlines the importance of Quaternary volcanism processes for interpreting $^{87}Sr/^{86}Sr$ data in paleomobility studies in volcanic regions.

1. Introduction

Strontium isotopes ($^{87}Sr/^{86}Sr$) are frequently used as chemical geographic tracers in archeological studies because unlike other isotopic systems, they are thought to be relatively stable in ecosystems over archeological times (Bentley, 2006; Montgomery, 2010). The $^{87}Sr/^{86}Sr$ primarily reflect those found in local bedrock units, which vary little at thousand-year timescales because they are controlled by the slow decay of ^{87}Rb into ^{87}Sr (Capo et al., 1998; Bataille and Bowen, 2012). The geological $^{87}Sr/^{86}Sr$ are propagated to local soil, plants and ecosystems (Flockhart et al., 2015), but the biologically available $^{87}Sr/^{86}Sr$ (bioavailable $^{87}Sr/^{86}Sr$) usually differs from that of local bedrock due to the mixing of Sr from isotopically distinct sources (Capo et al., 1998; Lewis et al., 2017). The successful application of this tracer for paleomobility studies requires to compare the isotopic ratio from the studied tissue to that of baselines able to predict the isotope ratio at a given

* Corresponding author.
** Corresponding author.
E-mail addresses: aserna@fcnym.unlp.edu.ar (A. Serna), cbataill@uottawa.ca (C.P. Bataille).

https://doi.org/10.1016/j.jas.2020.105198
Received 4 February 2020; Received in revised form 5 July 2020; Accepted 5 July 2020

location and time. Bioavailable $^{87}Sr/^{86}Sr$ datasets from plants, soils or local animals have multiplied over the last decade to capture this variability in archeologically-relevant regions of the globe under the assumption that modern samples are valid to develop $^{87}Sr/^{86}Sr$ baselines in archeological regions (e.g. Haverkort et al., 2008; Nafplioti, 2011; Frei, 2013; Hartman and Richards, 2014; Kootker et al., 2016; Barberena et al., 2017, 2019; Bataille et al., 2018; Ryan et al., 2018; Snoeck et al., 2018; Willmes et al., 2018; Lengfelder et al., 2019).

The bioavailable $^{87}Sr/^{86}Sr$ at a given location integrates a complex mixture of multiple non-local and non-geological isotopically-distinct sources (Bentley, 2006; Frei and Frei, 2011; Bataille et al., 2012; Fenner and Wright, 2014). Assessing and understanding their contributions at different timescale in controlling the bioavailable $^{87}Sr/^{86}Sr$ is critical for validating the use of $^{87}Sr/^{86}Sr$ isoscapes in paleomobility studies. Knowledge of the main controls of isotope propagation within a target region is also key to properly sample materials for bioavailable datasets and archeological studies (Crowley et al., 2017). Atmospheric deposition of sea salt and dust aerosols are among the processes that can modify the bioavailable $^{87}Sr/^{86}Sr$ at archeologically-relevant timescales (Capo et al., 1998; Montgomery, 2010). For example, as climate or sea-level changes at Quaternary timescales, the deposition of sea salt and dust in ecosystems will vary spatiotemporally and influence the local bioavailable $^{87}Sr/^{86}Sr$ in coastal regions (Evans et al., 2010) and downwind of desert zones (Bataille et al., 2012). The deposition and reworking of volcanic sediments and ash might be another potential source of bioavailable $^{87}Sr/^{86}Sr$ variability. Testing the potential of using $^{87}Sr/^{86}Sr$ to study human migration in the Maya Lowlands, Hodell et al. (2004) hypothesized that ash deposition and reworking could be generating local variations over the Yucatan Peninsula. As the deposition rate and transport of volcanic sediment can vary at Quaternary timescale, these processes could lead to some bioavailable $^{87}Sr/^{86}Sr$ variability relevant to archeological studies.

Río Negro Province (northern Patagonia, Argentina) represents an interesting location not only for paleomobility studies but also for testing the potential contribution of volcanos to the bioavailable $^{87}Sr/^{86}Sr$ variation in southern South America (Fig. 1). First, human interaction from different locations seems to have been intense during the late Holocene (Prates, 2008; Prates and Mange, 2016; Serna, 2018; Mange, 2019; Serna et al., 2019a, b). Second, this area shows complex geology with rock units having varied age and lithology (Fig. 1) (Ramos, 1984). Third, Río Negro is located downwind from major explosive volcanic centers (Stern, 2004) and it receives tephra and reworked loess transported by the dominant west winds. We aim to assess the dominant environmental and geological controls of bioavailable $^{87}Sr/^{86}Sr$ and to predict the isotopic variation across this area to build a high-resolution isoscape for provenance studies. We hypothesize that the bioavailable $^{87}Sr/^{86}Sr$ will be distinct from that of local geology and reflect, in part, the $^{87}Sr/^{86}Sr$ of volcanic products deposited in the region over time. For this purpose, we collected and analyzed $^{87}Sr/^{86}Sr$ in plant, soil and local fauna across the study area to represent the local bioavailable $^{87}Sr/^{86}Sr$. We then incorporated geological, climatic and environmental covariates into a tree-based regression (random forest) to assess the main controls of isotopic variation in this region. Finally, we applied spatially our model and create a bioavailable $^{87}Sr/^{86}Sr$ isoscape.

2. Materials and methods

2.1. Environmental and geological background

Río Negro (~203,000 km^2) is located at the northernmost Argentinian Patagonia and is crossed by the main fluvial systems of this region -the Negro and Colorado rivers- (Fig. 2) (Soldano, 1947; Spalletti and

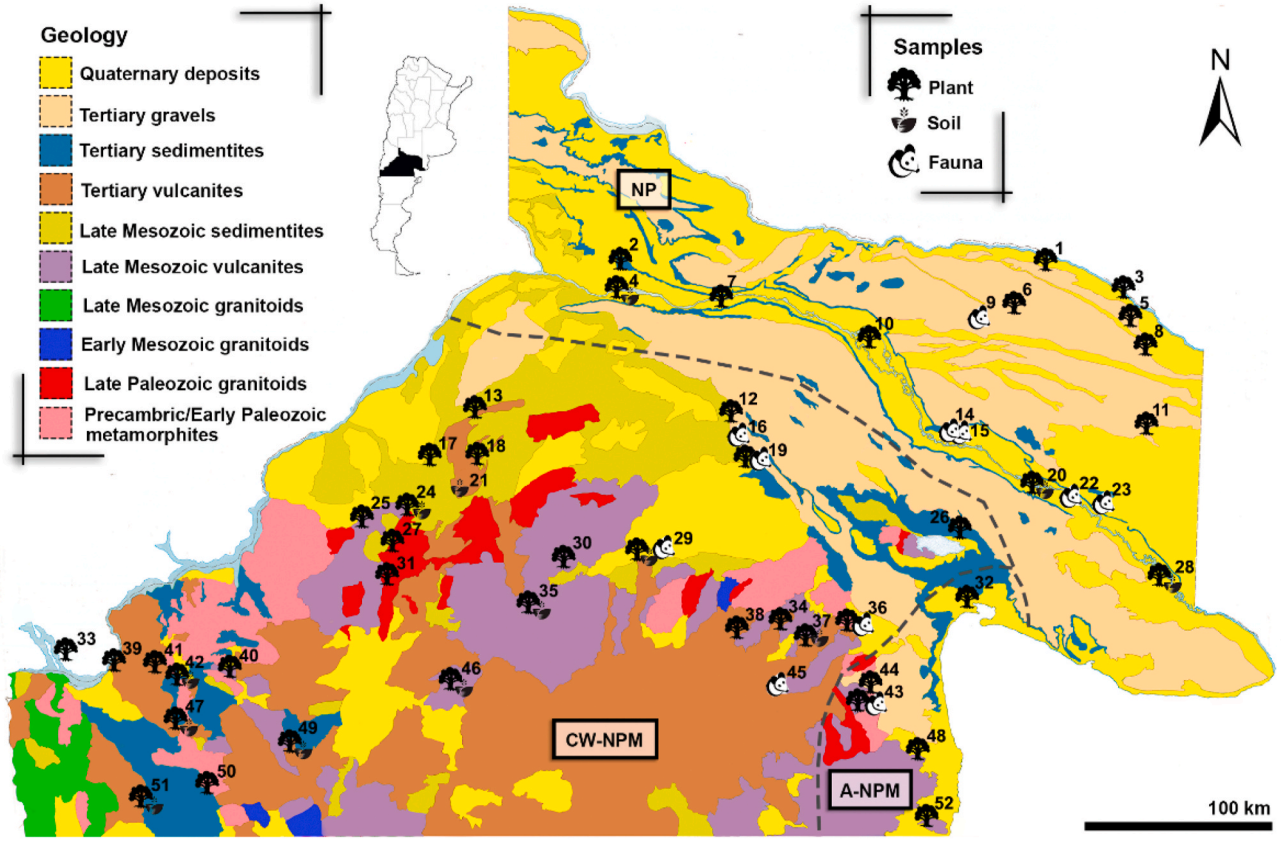

Fig. 1. Geological map of Río Negro Province showing the sample locations. The original map comes from the *Dirección Nacional del Servicio Geológico* (Argentina) and it was slightly simplified to achieve more uniform geological descriptions. Dashed lines divide sectors, CW-NPM: Central-west North Patagonian Massif; NP: Northern Plains; A-NPM: Atlantic North Patagonian Massif. The numbers on the map correspond with the locations in Table 1.

Isla, 2003). This area is located within the belt of westerlies, so that is affected by the Pacific anticyclone with discrete intrusions of humid air masses from the Atlantic Ocean (Paruelo et al., 1998; Iriondo, 2000). Predominant west winds -westerlies- are intercepted by the Andes, resulting in arid/semi-arid conditions in most of the area and a landscape that gradually changes from forest in the West to different kinds of steppes eastward (Paruelo et al., 1998; Schäbitz, 2003). The topography of Río Negro is complex and varies from West to East (Fig. 2). At the extreme West, a north-to-south mountain range placed by the Andean tectonics rises, while eastward hill ranges appear irregularly to reach the plateaus of the Somuncurá Massif and, finally, the Atlantic coast (Fidalgo and Rabassa, 1984). The north is dominated by plains and it is intersected by river valleys. The soils of Río Negro present a neutral to alkaline pH and are dominated by Aridisols (on the top of plains, plateaus and depressions); while river valleys are dominated by Entisols (Luchsinger, 2006; Godagnone et al., 2010).

Geologically, Río Negro is divided into three sectors: Northern Plains, Central-west North Patagonian Massif and Atlantic North Patagonian Massif (González Díaz and Malagnino, 1984; Basei et al., 2005) (Fig. 1). The Northern Plains sector is the youngest and most geologically homogeneous. On the surface, it presents partially carbonated Quaternary aeolian deposits that lie over the Pliocene-Pleistocene conglomerates of the Rodados Patagónicos Formation (Folguera and Zárate, 2009; Martínez et al., 2009; Escosteguy et al., 2011) underlined by the Cenozoic blue-grey sandstones from the Río Negro Formation (Franchi et al., 1984; Escosteguy et al., 2011). The Central-west North Patagonian Massif sector is the most geologically diverse and its basement comprises a mixture of metamorphic and igneous rocks of varied ages (Basei et al., 2005). Late Paleozoic granitoids cover a large part of the western edge of the North Patagonian Massif (Varela et al., 2005; Pankhurst et al., 2006). These plutonic and metamorphic rock units are widely covered by Triassic ignimbrites (Los Menucos Complex), Cretaceous sedimentary formations (Neuquén Group) and Cenozoic basaltic plateaus (e.g. Somuncurá, Cari Laufquen, Coli Toro and El Cuy) (Cucchi et al., 2001; Hugo and Leanza, 2001). The Atlantic North Patagonian Massif sector presents the oldest geologic formations in the region dated to Precambrian-Early Paleozoic (e.g. El Jagüelito, Nahuel Niyeu, Mina Gonzalito complex, Arroyo Salado, Sierra Grande), with high (gneiss) to low (schists) grade metamorphic rocks intruded by post-tectonic granite stocks covered by a deformed Silurian sedimentary sequence (Basei et al., 2005; Pankhurst et al., 2006). The predominantly rhyolitic Marifil Formation (Jurassic silicic Province of Chon Aike) covering more than 10,000 km^2 overlays these rock units, especially in the southern portion of the sector (Pankhurst et al., 1998; Martínez and Rabassa, 2014).

2.1.1. *Atmospheric deposition: Mineral aerosol and volcanism*

Patagonia region is the major dust supplier across South America (Iriondo, 2000; Prospero et al., 2002). Low precipitation and poor vegetation coverage enhance the occurrence of mineral aerosol transport mostly triggered by the westerlies (Gaiero et al., 2003, 2004). Río Negro is also part of the Southern Volcanic Zone of the Andes (~33° - 46°S), a continuous volcanic arc segment -~1400 km long-that arises from the subduction of the oceanic Nazca Plate beneath the continental South American Plate (Stern, 2004). Although almost every volcanic center is on the western margin of the Andes in Chile, the latitudes in which Río Negro is located (~37° - 42°S) comprises several active volcanoes that have been depositing materials into the region since the Late Quaternary (e.g. Gaiero et al., 2007; Fontijn et al., 2014, 2016; Hickey-Vargas et al., 2016).

Dust and surficial sediments covering continental Patagonia come primarily from volcanic sources, including reworked sediments from the Jurassic silicic Province of Chon Aike and Quaternary sediments from southern Andean volcanism (Gaiero et al., 2007; Gili et al., 2017). In northeastern Patagonia, the sediment loads from the main rivers (Negro and Colorado) are water-transported products from the erosion of Quaternary Andean volcanic material and Andean bedrock, which are deposited on floodplains and reworked by aeolian action (Blasi and Manassero, 1990; Zárate and Blasi, 1993; Zárate, 2003). The direct input of tephra to soils by frequent Andean eruptions and strong westerlies has also been a relevant process during the Holocene (Zárate and Blasi, 1993; Zárate, 2003; Villarosa et al., 2006; Gaiero, 2007; Amigo et al., 2013; Watt et al., 2013). Recently, the most salient volcanic ash falls over Río Negro were from Chaitén in 2008, Puyehue-Cordón Caulle

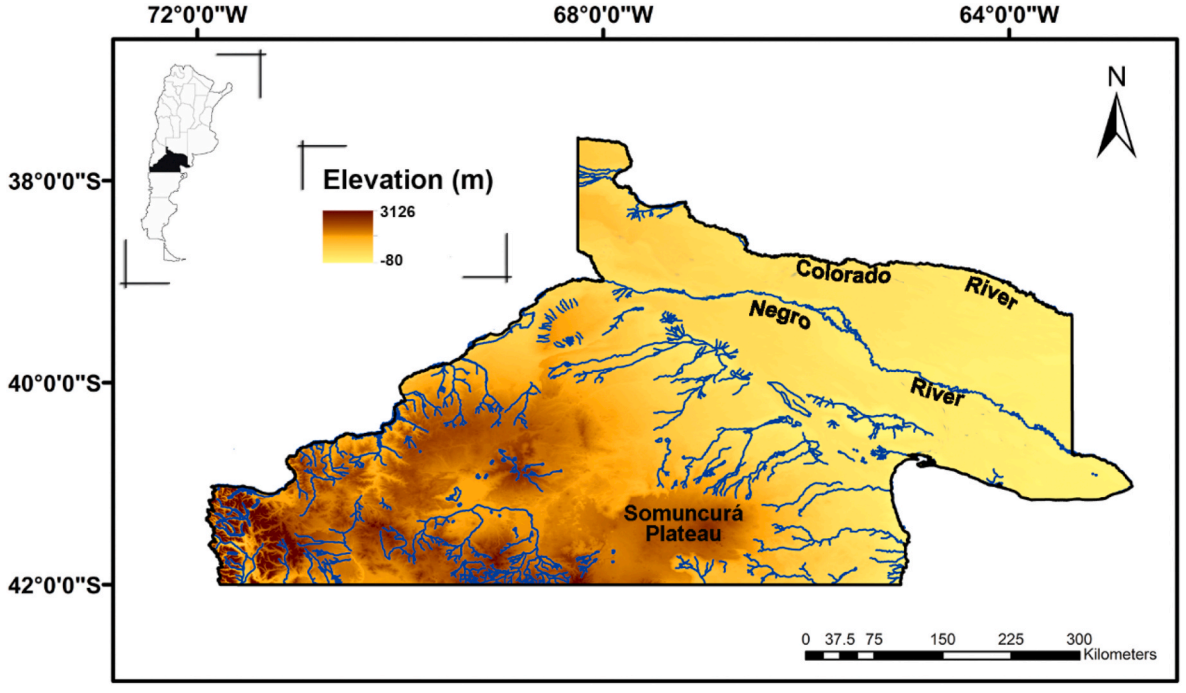

Fig. 2. Digital elevation model with the drainage system of the study area (data from *Instituto de Geología y Recursos Minerales. SEGEMAR. Argentina*).

Table 1
Spatial, geological and isotopic data of the analyzed samples. P–F, P–S and S–F show the results from the subtractions of the $^{87}Sr/^{86}Sr$ ratios of different kinds of samples from the same location. Location refers to Fig. 1. CW-NPM: Central-west North Patagonian Massif; NP: Northern Plains; A-NPM: Atlantic North Patagonian Massif.

Sector	Location	Latitude	Longitude	Geology	ID	Sample	$^{87}Sr/^{86}Sr$	±2σ	P–F	P–S	S–F
CW-NPM	12	−39.707	−66.896	Cretaceous sedimentary/igneous	UCT-18951	Plant	0.70679	0.00001	–	–	–
					UCT-18952	Plant	0.70704	0.00001	–	–	–
	13	−39.727	−68.510	Cenozoic sedimentary/igneous	IGGRC-15035	Plant	0.70637	0.00004	–	–	–
	16	−39.827	−66.863	Cretaceous sedimentary/igneous	UCT-18939	Fauna	0.70676	0.00001	–	–	–
	17	−39.950	−68.831	Cretaceous sedimentary/igneous	IGGRC-15062	Plant	0.70653	0.00002	–	–	–
	18	−39.977	−68.430	Cenozoic sedimentary/igneous	IGGRC-15042	Plant	0.70592	0.00002	–	–	–
	19	−39.989	−66.643	Cretaceous sedimentary/igneous	IGGRC-15031	Plant	0.70640	0.00001	0.00012	–	–
					UCT-18935	Fauna	0.70625	0.00002	–	–	–
					UCT-18937	Fauna	0.70635	0.00002	–	–	–
					UCT-18938	Fauna	0.70623	0.00001	–	–	–
	21	−40.145	−68.603	Cenozoic sedimentary/igneous	IGGRC-15055	Soil	0.70617	0.00001	–	–	–
	24	−40.237	−68.966	Paleozoic metamorphic/igneous	IGGRC-15054	Soil	0.70585	0.00002	–	0.00028	–
					IGGRC-15087	Plant	0.70613	0.00001	–	–	–
	25	−40.343	−69.147	Triassic igneous	IGGRC-15045	Plant	0.70619	0.00001	–	–	–
	26	−40.375	−65.033	Cenozoic sedimentary/igneous	UCT-18950	Plant	0.70711	0.00001	–	–	–
	27	−40.465	−69.059	Paleozoic metamorphic/igneous	IGGRC-15030	Plant	0.70601	0.00008	–	–	–
					IGGRC-15038	Plant	0.70578	0.00002	–	–	–
	29	−40.501	−67.227	Cenozoic sedimentary/igneous	IGGRC-15056	Plant	0.70632	0.00000	0.00017	0.00034	0.00050
					IGGRC-15074	Soil	0.70598	0.00002	–	–	–
					IGGRC-15080	Fauna	0.70649	0.00001	–	–	–
	30	−40.591	−67.766	Triassic igneous	IGGRC-15084	Plant	0.70599	0.00000	–	–	–
	31	−40.671	−69.108	Paleozoic metamorphic/igneous	IGGRC-15043	Plant	0.70570	0.00002	–	–	–
					IGGRC-15060	Plant	0.70567	0.00002	–	–	–
					IGGRC-15090	Plant	0.70567	0.00001	–	–	–
	33	−40.783	−71.627	Cretaceous sedimentary/igneous	IGGRC-15046	Plant	0.70461	0.00002	–	–	–
					IGGRC-15066	Plant	0.70522	0.00001	–	–	–
	34	−40.838	−66.300	Cenozoic sedimentary/igneous	IGGRC-15041	Plant	0.70638	0.00003	–	–	–
	35	−40.841	−68.090	Triassic igneous	IGGRC-15073	Plant	0.70648	0.00001	–	0.00019	–
					IGGRC-15082	Soil	0.70629	0.00001	–	–	–
	36	−40.850	−65.849	Cenozoic sedimentary/igneous	IGGRC-15050	Plant	0.70770	0.00001	0.00019	–	–
					UCT-18957	Plant	0.70704	0.00001	–	–	–
					IGGRC-15051	Fauna	0.70704	0.00002	–	–	–
					UCT-19068	Fauna	0.70721	0.00001	–	–	–
					UCT-19069	Fauna	0.70724	0.00002	–	–	–
					UCT-19070	Fauna	0.70720	0.00001	–	–	–
	37	−40.852	−65.878	Cenozoic sedimentary/igneous	IGGRC-15040	Plant	0.70775	0.00000	–	0.00088	–
					IGGRC-15075	Soil	0.70687	0.00001	–	–	–
	38	−40.957	−66.637	Cenozoic sedimentary/igneous	IGGRC-15063	Plant	0.70575	0.00001	–	–	–
	39	−41.056	−71.149	Cenozoic sedimentary/igneous	IGGRC-15033	Plant	0.70561	0.00002	–	–	–
					IGGRC-15064	Plant	0.70764	0.00002	–	–	–
	40	−41.071	−70.337	Paleozoic metamorphic/igneous	IGGRC-15049	Plant	0.70466	0.00001	–	–	–
					IGGRC-15072	Plant	0.70608	0.00001	–	–	–
	41	−41.090	−70.830	Cenozoic sedimentary/igneous	IGGRC-15048	Plant	0.70467	0.00001	–	–	–
					IGGRC-15067	Plant	0.70468	0.00002	–	–	–
	42	−41.121	−70.717	Cenozoic sedimentary/igneous	IGGRC-15044	Plant	0.70467	0.00001	–	0.00000	–
					IGGRC-15057	Soil	0.70465	0.00002	–	–	–
					IGGRC-15086	Plant	0.70463	0.00001	–	–	–
	45	−41.214	−66.338	Cenozoic sedimentary/igneous	IGGRC-15068	Fauna	0.70626	0.00000	–	–	–
					UCT-18929	Fauna	0.70643	0.00001	–	–	–
	46	−41.269	−68.759	Triassic igneous	IGGRC-15036	Plant	0.70576	0.00001	–	0.00003	–
					IGGRC-15069	Soil	0.70574	0.00001	–	–	–
	47	−41.289	−70.702	Cenozoic sedimentary/igneous	IGGRC-15070	Plant	0.70477	0.00001	–	–	–
	49	−41.489	−69.785	Cenozoic sedimentary/igneous	IGGRC-15039	Plant	0.70583	0.00000	–	0.00014	–
					IGGRC-15077	Soil	0.70569	0.00002	–	–	–
	50	−41.777	−70.432	Paleozoic metamorphic/igneous	IGGRC-15079	Plant	0.70507	0.00007	–	–	–
	51	−41.801	−70.796	Cenozoic sedimentary/igneous	IGGRC-15052	Soil	0.70476	0.00002	–	0.00062	–
					IGGRC-15059	Plant	0.70538	0.00003	–	–	–
NP	1	−38.895	−64.457	Cenozoic sedimentary/igneous	UCT-18947	Plant	0.70700	0.00002	–	–	–
	2	−38.903	−67.582	Cenozoic sedimentary/igneous	IGGRC-15088	Plant	0.70689	0.00001	–	–	–
	3	−39.015	−64.133	Quaternary sediment	UCT-18944	Plant	0.70670	0.00002	–	–	–
	4	−39.108	−67.627	Quaternary sediment	IGGRC-15032	Plant	0.70659	0.00001	–	0.00001	–
					IGGRC-15089	Soil	0.70659	0.00003	–	–	–
	5	−39.115	−64.020	Cenozoic sedimentary/igneous	IGGRC-15083	Plant	0.70679	0.00009	–	–	–
	6	−39.129	−64.828	Cenozoic sedimentary/igneous	IGGRC-15037	Plant	0.70674	0.00003	–	–	–
	7	−39.148	−66.717	Quaternary sediment	UCT-18948	Plant	0.70642	0.00001	–	–	–
	8	−39.161	−64.017	Cenozoic sedimentary/igneous	UCT-18941	Plant	0.70715	0.00001	–	–	–
					UCT-18942	Plant	0.70715	0.00001	–	–	–
					UCT-18943	Plant	0.70654	0.00001	–	–	–
	9	−39.231	−65.117	Cenozoic sedimentary/igneous	UCT-18940	Fauna	0.70675	0.00001	–	–	–
	10	−39.346	−65.745	Quaternary sediment	UCT-18945	Plant	0.70603	0.00001	–	–	–
					UCT-18946	Plant	0.70595	0.00001	–	–	–
	11	−39.605	−63.784	Cenozoic sedimentary/igneous	IGGRC-15065	Plant	0.70687	0.00000	–	–	–
	14	−39.813	−65.312	Quaternary sediment	UCT-18927	Fauna	0.70613	0.00001	–	–	–

(continued on next page)

Table 1 (*continued*)

Sector	Location	Latitude	Longitude	Geology	ID	Sample	$^{87}Sr/^{86}Sr$	±2σ	P–F	P–S	S–F
	15	−39.817	−65.284	Quaternary sediment	UCT-18928	Fauna	0.70609	0.00001	–	–	–
	20	−40.104	−64.473	Quaternary sediment	IGGRC-15034	Plant	0.70635	0.00001	–	0.00027	–
					IGGRC-15053	Soil	0.70662	0.00008	–	–	–
	22	−40.146	−64.272	Quaternary sediment	UCT-18867	Fauna	0.70614	0.00001	–	–	–
					UCT-18869	Fauna	0.70614	0.00001	–	–	–
	23	−40.169	−64.142	Quaternary sediment	UCT-18868	Fauna	0.70670	0.00002	–	–	–
	28	−40.490	−63.690	Quaternary sediment	IGGRC-15071	Soil	0.70627	0.00015	–	0.00017	–
					IGGRC-15076	Plant	0.70625	0.00002	–	–	–
					IGGRC-15081	Plant	0.70596	0.00003	–	–	–
A-NPM	32	−40.711	−65.004	Quaternary sediment	IGGRC-15047	Plant	0.70728	0.00000	–	–	–
	43	−41.131	−65.718	Paleozoic metamorphic/igneous	UCT-18953	Plant	0.70667	0.00001	–	–	–
					UCT-18955	Plant	0.70651	0.00001	–	–	–
					UCT-18956	Plant	0.70663	0.00002	–	–	–
	44	−41.158	−65.792	Jurassic igneous	IGGRC-15078	Fauna	0.70672	0.00001	0.00069	–	–
					UCT-18932	Fauna	0.70672	0.00001	–	–	–
					UCT-18933	Fauna	0.70821	0.00001	–	–	–
					UCT-18934	Fauna	0.70762	0.00001	–	–	–
					UCT-18954	Plant	0.70663	0.00002	–	–	–
	48	−41.426	−65.358	Jurassic igneous	IGGRC-15085	Plant	0.70711	0.00000	–	–	–
	52	−41.999	−65.289	Jurassic igneous	IGGRC-15058	Plant	0.70785	0.00001	–	–	–
					IGGRC-15061	Plant	0.70769	0.00000	–	–	–
	$N = 52$						$N = 94$				

complex in 2011 and a very small contribution from Calbuco in 2015 (Watt et al., 2009; Alloway et al., 2015, 2017; Romero et al., 2016). Due to the explosive eruption of Puyehue Cordón-Caulle, 97% of the study area (~197,000 km^2) experienced tephra depositions (Gaitán et al., 2011).

2.2. Sample collection and analytical methods

We sampled 52 locations all over the study area during the year 2016, and analyzed 94 samples: fauna ($n = 21$), soils ($n = 12$) and plants ($n = 61$) (Fig. 1; Table 1). All the samples were taken from carefully selected locations that are distant from any anthropogenic activities including farming. The fauna sample comprises the teeth of small-sized mammals with local ranges of action (mostly rodents) found in stratigraphic position or nearby archeological contexts. Since there is no protocol to effectively separate the enamel from the dentine, the latter more sensitive to diagenesis, we prioritized the selection of teeth with a high amount of enamel in relation to dentine (e.g. incisors) to avoid mixed ratios. We took top soil samples representing approximately the first 5 cm of the soil profile. We selected that depth to avoid pre-Holocene sediments and because most archeological deposits of the study area are palimpsests located within or on the top of fluvial-aeolian sediments from the Holocene (Gaiero et al., 2003: Luchsinger, 2006; Prates, 2008). The samples were mostly sandy to fine-grain Aridisol and Entisol, and they were sampled in close distance to the plants. The sampling of plants was focused on the most represented plant groups in the arid/semi-arid northern Patagonia (e.g. shrubs as *Larrea* sp.), in which the highest root activity occurs in the upper soil (Rodríguez et al., 2007). Each plant sample is composed of the bulk of three plants of the same species or root depth which were collected within a small distance radius.

Samples were prepared and analyzed at the Department of Geology of the University of Cape Town (UCT) and the Ottawa-Carleton Isotope Geochemistry and Geochronology Research Center (IGGRC). We followed with minor modifications the protocols of Villalba-Mouco et al. (2018) for small mammals and by Willmes et al. (2014) for soil and plant.

Faunal samples (teeth) were cleaned by abrasion, rinsed and ultrasonicated for 2 h in MilliQ water. To remove any organic matter and diagenetic carbonate phases they were washed in 0.5 mL of 12.3 M hydrogen peroxide (H_2O_2) overnight and then with 2 mL of 0.1 M nitric acid (HNO_3) for 2 h, respectively. A ~50 mg of sample was digested in 7 mL Savillex PTFE vials with 2 mL of concentrated HNO_3 at 140 °C for an hour.

Each dry soil sample (30 g) was homogenized avoiding large pieces of plant material by sieving them (2 mm). A 1 g aliquot was subsampled and leached by adding 5 mL of 0.4 M HNO_3 and ultrasonicated for 2 h. This weak acid procedure can remove Sr from the exchange complex (i.e. clay and organic matter) and is similar to the extraction using ammonium acetate buffer (Beard and Johnson, 2000). Samples were then centrifuged at 3000 rpm for 10 min, ~2 mL were extracted, evaporated at 80 °C and, finally, re-dissolved in 1 mL 2 M HNO_3.

Plant samples were first washed in double deionized water in an ultrasonic bath for 30 min. Samples were then dried at 50 °C in a drying oven and ashed in porcelain crucible (800 °C for 8 h). Once ashed, the samples were transferred to 7 mL Teflon vials and further digested in a mixture of ≥12.3 M H_2O_2 (TraceMetal Grade; Sigma-Aldrich) and concentrated nitric acid (16 M) (Distilled TraceMetal Grade; Fisher Chemical) for 48 h at 150 °C.

After digestion or leaching, samples were dried on a hot plate at 70 °C and re-dissolved in 5 mL of 0.4 M HNO_3 and divided into two aliquots: (1) a 0.1 mL aliquot for Sr concentration analysis, and (2) the remaining aliquot was used for $^{87}Sr/^{86}Sr$ analysis. The Sr concentration analysis was performed by Inductively Coupled Plasma Mass Spectrometry (ICP-MS, ICP-QQQ Agilent 8800) at the University of Ottawa. In both laboratories (UCT and IGGRC), the Sr was purified with a similar protocol using gravity chromatography columns filled with Eichrom Sr-spec Resin (100–150 μm). The separated fraction for each sample was dried down, dissolved in 2 mL of 0.04 M distilled HNO_3 and diluted to 200 ppb Sr concentrations for isotope analysis in a NuPlasma HR MC-ICP mass spectrometer (UCT) and Neptune MC-ICP-MS (IGGRC). Sample analyses were referenced to bracketing analyses of SRM987 with analytical precision of 0.000035 (2σ, $n = 33$; UCT) and 0.0000163 (2σ, $n = 25$; IGGRC).

2.3. Statistical procedures

All statistical analyses were conducted in R 3.5.3 (https://cran.r-project.org/). The bioavailable $^{87}Sr/^{86}Sr$ was described via Tukey's IQR boxplot method by type of sample and by geology. To examine the isotopic differences by geographic location, the non-parametric tests Kruskal-Wallis and -Bonferroni corrected- Wilcoxon rank-sum for multiple pairwise comparisons were conducted under a signification level of 0.05 (Zar, 1999). Prior to using the random forest regression, we generated a bedrock $^{87}Sr/^{86}Sr$ isoscape for the study area by applying the predictive model of Bataille et al., (2014) (see Text S1). Briefly, this

Table 2
Covariates tested in the random forest regression (see also Text S1 and Table S1).

Covariate	Description	Resolution	Source
r.m1	Median bedrock model	1 km	Bataille et al. (2014)
r.XX	GLiM 1st lithological class attribute	1 km	Hartmann and Moosdorf (2012)
r.Age	Terrane age attribute	1 km	Mooney et al. (1998)
r.salt	CCSM.3 simulation	1.4° × 1.4°	Mahowald et al. (2006)
r.dust	Multi-models average	1° × 1°	Mahowald et al. (2006)
r.elevation	SRTM	90 m	Jarvis et al. (2008)
r.ph	Soil pH in H_2O solution	250 m	Hengl et al. (2017)
r.clay	Clay (weight %)	250 m	Hengl et al. (2017)
r.map	Mean annual precipitation (mm.yr^{-1})	30-arc sec	Hijmans et al. (2005)

method uses bedrock age and lithology from the global lithological map (GLiM, Hartmann and Moosdorf, 2012) to predict $^{87}Sr/^{86}Sr$ variation in rocks. To compare the bioavailable $^{87}Sr/^{86}Sr$ with local geology, we subtracted the observed bioavailable $^{87}Sr/^{86}Sr$ with the predicted $^{87}Sr/^{86}Sr$ in rocks at the same location (noted as $\Delta^{87}Sr/^{86}Sr_{(S\text{-}BRm)}$).

We then used the random forest regression framework developed by Bataille et al. (2018) to assess the main predictors of bioavailable $^{87}Sr/^{86}Sr$ variation in the study area (see R base script in Bataille et al., 2018). The method uses a machine-learning approach to assess the most important predictors among a series of geological, climatological, topographic and environmental covariates (see the details in Text S1). In a first step, we use the geographic location of each sample to extract geological, climatological, topographic and environmental conditions at each sampling site using high-resolution geospatial products (Table 2; Table S1). In a second step, we used the collated regression matrix to train a model using 10-fold cross-validation implemented using the *caret* package (Kuhn, 2008). We optimized the selection of significant predictors by using the *Variable Selection Using Random Forest* package (Genuer et al., 2015). The RMSE (root mean square error) was used as the main performance metric to tune the bioavailable $^{87}Sr/^{86}Sr$ model.

3. Results and discussion

3.1. Bioavailable $^{87}Sr/^{86}Sr$ data

The $^{87}Sr/^{86}Sr$ of the whole dataset range from 0.7046 to 0.7082 with a median of 0.7064 and a mean of 0.7063 ± 0.0008 ($N = 94$) (Table 1). When collected at the same location, different types of samples show little difference (<0.0003 for Plant vs. Fauna and Plant vs. Soil on average, and <0.0005 for Soil vs. Fauna) with an average difference per location of 0.0003 (Table 1). The statistical summaries by type of sample and geological units are presented in Table S2. The observed bioavailable $^{87}Sr/^{86}Sr$ does not fit with the $^{87}Sr/^{86}Sr$ of underlying geological units. Although the dataset includes samples collected across a wide range of geologic ages, most of the $^{87}Sr/^{86}Sr$ fall into a narrow range typical of young mafic rocks (0.7046–0.7077) (Fig. 3). In the CW-NPM, samples collected on the oldest geological unit (Paleozoic) have lower ratios than samples collected on younger Triassic and Cretaceous units from this same sector. Similarly, in the A-NPM, the lowest ratios are found in samples collected on the oldest geological units. In the NP, there is a spacing between samples from Cenozoic and Quaternary geological units, where the former presents the highest ratios (Fig. 3; Table S2). The medians of the three sectors differ significantly (Kruskal-Wallis; $H = 20.437$, $p = 0.00004$) and all sectors differ among themselves (Multiple pairwise comparisons; NP vs. A-NPM $p = 0.01045$; NP vs. CW-NPM $p = 0.02646$, and CW-NPM vs. A-NPM $p = 0.00025$). However, the difference among these sectors does not follow a predictable pattern following rock age and lithology as would be expected if bedrock was the dominant control of bioavailable $^{87}Sr/^{86}Sr$ variation (see section 2.1).

3.2. Bioavailable vs bedrock model $^{87}Sr/^{86}Sr$ data

If bedrock was the dominant control of bioavailable $^{87}Sr/^{86}Sr$, we would expect a wide range of variation (from ~0.7030 to >0.8000; Dalla Salda et al., 1994; Pankhurst and Rapela, 1995; Pankhurst et al., 1998; Varela et al., 2009, 2014), and more radiogenic ratios in the older geological units in the South and a decrease northward, where younger sedimentary units dominate (section 2.1). Compared with the predicted bedrock $^{87}Sr/^{86}Sr$ across the study area (0.7030–0.7180), the bioavailable $^{87}Sr/^{86}Sr$ exhibits a narrower range of variation (0.7046–0.7082) (Fig. 4; Table S3). The progressive increase from the Southwest to the Northeast in the bioavailable $^{87}Sr/^{86}Sr$ from samples also differs from that observed in the bedrock model (Fig. 4A). Differences between the $^{87}Sr/^{86}Sr$ of the samples and the bedrock ($\Delta^{87}Sr/^{86}Sr_{(S\text{-}BRm)}$) are > 0.001 in 85% of the locations (Fig. 4B), with the maximum and minimum

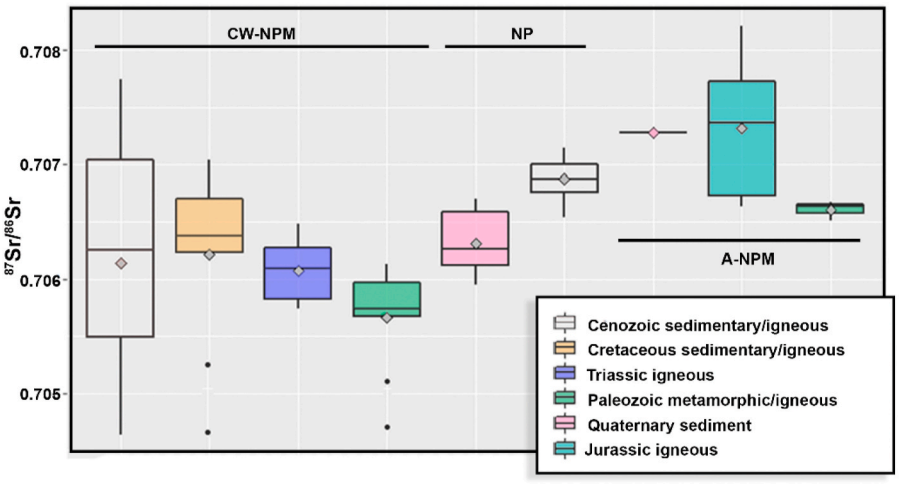

Fig. 3. Variation of $^{87}Sr/^{86}Sr$ in the analyzed dataset by geology. In the boxplot, the middle line is the median value and the lower and upper bounding boxes are the lower and upper quartiles, respectively. The lines extending from the boxes indicate variability outside the upper and lower quartiles. Outliers are plotted as individual points. Grey diamonds represent the mean values. CW-NPM: Central-west North Patagonian Massif; NP: Northern Plains; A-NPM: Atlantic North Patagonian Massif.

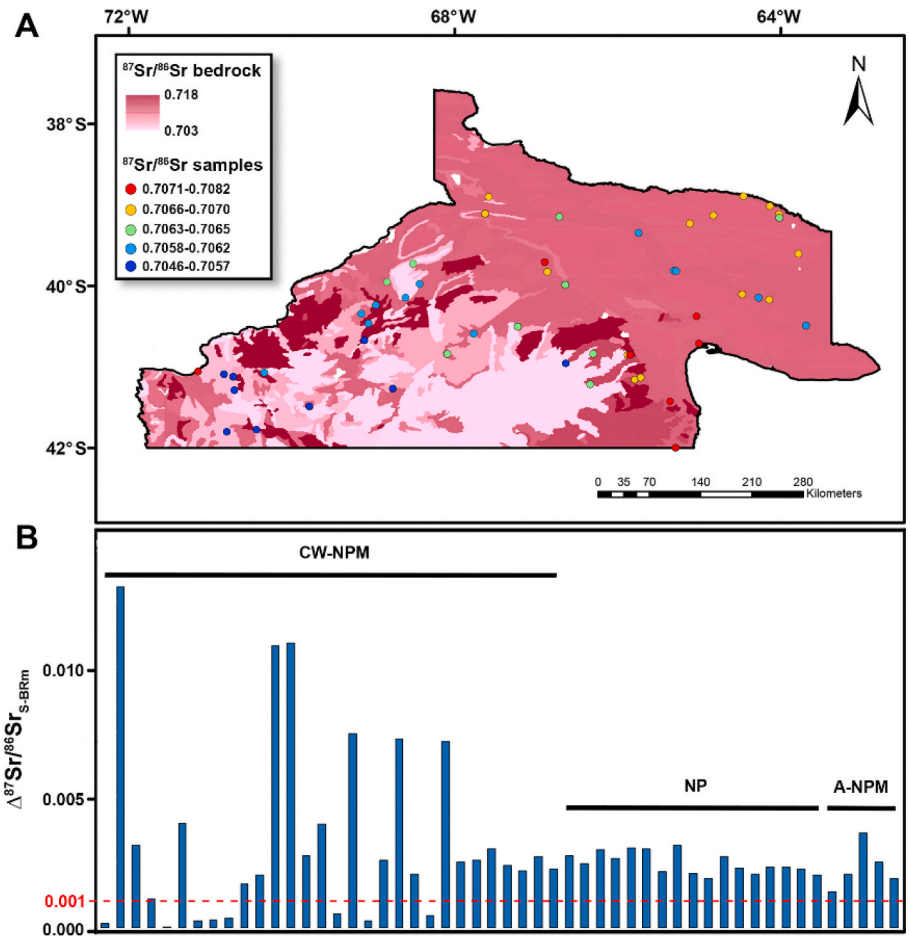

Fig. 4. Differences in $^{87}Sr/^{86}Sr$ between samples and bedrock model (see also Table S3). A. Bedrock isoscape according to Bataille et al., (2014) predictive model with the ratios of the analyzed samples; B. Barplot showing the subtractions in absolute value between samples and predicted bedrock values at each sampled location. The dashed red line highlights the differences above the third decimal. Horizontal bars refer to geological sectors: CW-NPM: Central--west North Patagonian Massif; NP: Northern Plains; A-NPM: Atlantic North Patagonian Massif. (For interpretation of the references to colour in this figure legend, the reader is referred to the Web version of this article.)

values being 0.013 and 0.000006, respectively. It is worth noting that CW-NPM exhibits both the highest (>0.007, $n = 6$) and the smallest differences (<0.0005, $n = 8$) (Fig. 4B).

The consistent difference between the $^{87}Sr/^{86}Sr$ of geological units and the collected samples across the study area suggests that ecosystems in Río Negro receive Sr inputs from other sources than bedrock. Besides the action of some processes occurring within the soil (e.g. differential mineral weathering, precipitation of secondary minerals and mixing with organic matter, Hajj et al., 2017), atmospheric inputs can also act as a relevant source of Sr for the lithosphere and biosphere (e.g. Graustein, 1989; Hartman and Richards, 2014).

3.3. The random forest regression model

The n-fold cross-validated random forest regression explains 71% of the variance ($R^2 = 0.71$) with an RMSE of 0.00041 using only dust deposition and elevation as predictors (Fig. 5A). The residuals are centered on zero with a larger dispersion around higher $^{87}Sr/^{86}Sr$ (Fig. S1) indicating higher predictive uncertainties in sectors with more radiogenic ratios such as A-NPM (see section 3.4). As previously demonstrated (Bataille et al., 2018), the random forest is capable of fitting highly accurate and precise models for bioavailable $^{87}Sr/^{86}Sr$ variation in different environments. Our results show that only geographic and environmental covariates, dust aerosol deposition (r. dust) and elevation (r.elevation), are required to predict the bioavailable $^{87}Sr/^{86}Sr$ variations across Río Negro (Fig. 5B). Geology-related variables such as lithology, geological age or predictions from the bedrock model are not significant predictors. The partial dependence plot shows that the $^{87}Sr/^{86}Sr$ increase as the dust deposition increases and they decrease at higher altitudes (Fig. 5C).

3.4. Bioavailable $^{87}Sr/^{86}Sr$ isoscape

In spite of the broad geological variation, the range of $^{87}Sr/^{86}Sr$ among ecosystems throughout Río Negro is relatively narrow (~0.7040–0.7070) (Fig. 6). Local bedrock units seem to have played little role in controlling exchangeable Sr of soils likely because the arid climate limits the erosion and weathering of local bedrock by water (Blisniuk et al., 2005). Rather, most sediments forming Patagonia top soils originate from atmospheric deposition sources (Gaiero et al., 2007). Massive volumes of volcaniclastic sediments are produced in the Andes where steep slopes and heavy rainfall facilitate their physical erosion and transport (Gaiero et al., 2007). Nowadays only a small amount of those volcaniclastic sediments are transported by eastward flowing rivers towards the continental interiors of the Patagonian Plateau but glaciers transported much larger volume of sediments in the Last Glacial Maximum (Gaiero et al., 2002, 2003). These sediments were deposited westward and remobilized by wind and fluvial erosion throughout the study area (Coronato et al., 2004). Active basaltic to andesitic volcanism from the Andes also produces a large amount of tephra, which is transported by the dominant westerlies winds and redeposited throughout the region (Stern, 2004). The low-density loess and tephra combined with the arid conditions of inland Patagonia facilitate the regional reworking and re-deposition of volcaniclastic sediments by wind homogenizing bioavailable $^{87}Sr/^{86}Sr$ (Panebianco et al., 2017). The weathering of those sediments forms clay-rich volcanic soils with a narrow range of $^{87}Sr/^{86}Sr$ variation in comparison to the underlying geological units across Río Negro (Fig. 4). The geochemistry of those soils and plants reflect, therefore, a dominance of Quaternary Andean volcaniclastic material. For example, in the last 20 years, at least three major eruptions (Calbuco, Chaitén and Puyehue-Cordón Caulle

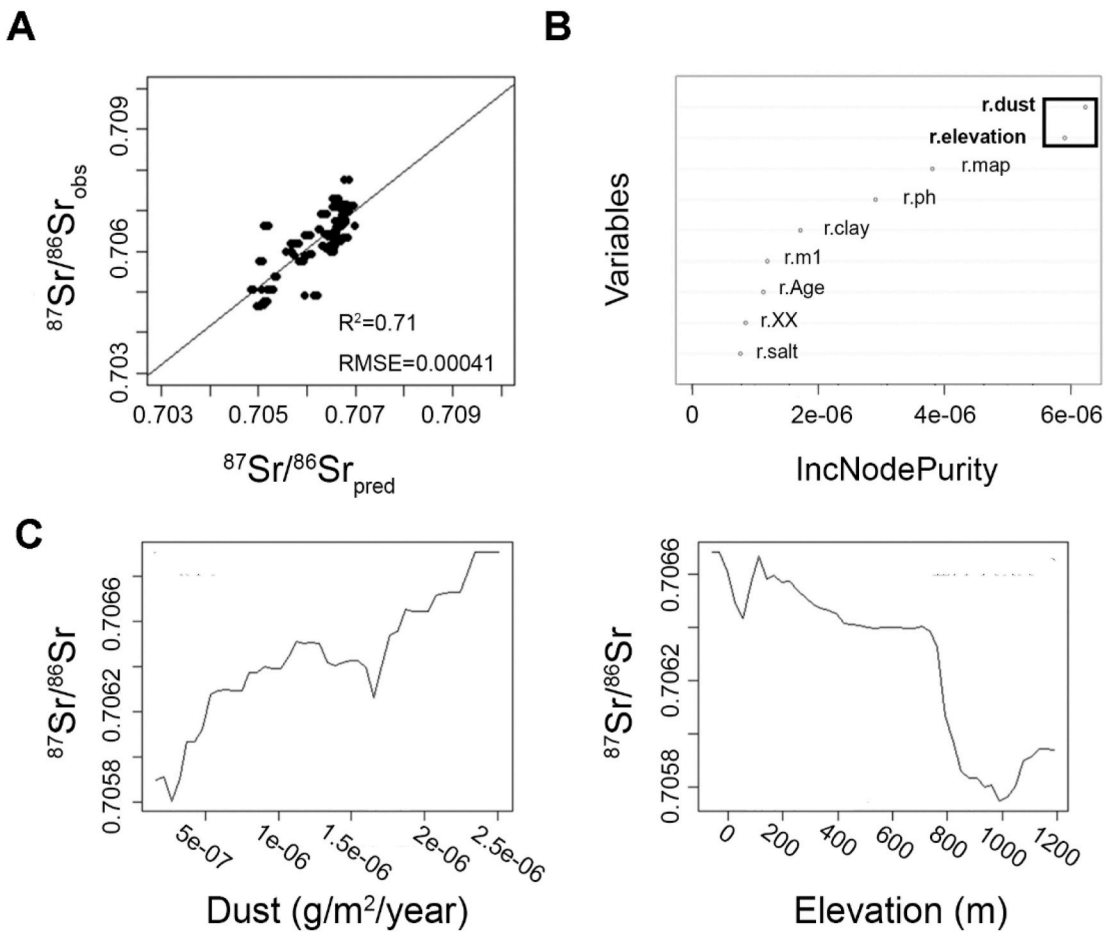

Fig. 5. Random forest regression results. A. Observed vs. predicted $^{87}Sr/^{86}Sr$ over the five times 10-fold cross-validation testing dataset. R^2 = coefficient of determination; RMSE = root mean square error. B. Variable importance plot showing the selected variables -inset- by VSURF (see Table 2 for the description of variables). C. Partial dependence plots for the most relevant variables.

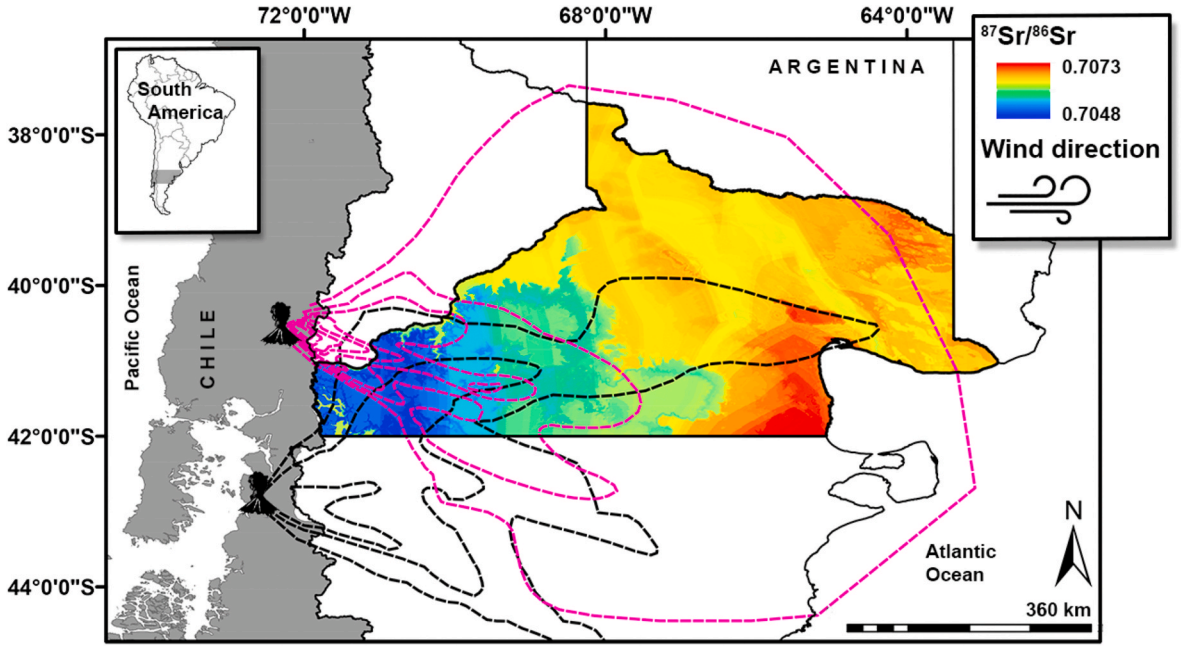

Fig. 6. Bioavailable $^{87}Sr/^{86}Sr$ isoscape of Río Negro. Dashed lines represent isopachs from recent volcanic eruptions: Chaitén 2008 in black and Puyehue-Cordón Caulle 2011 in pink (see the details of the isopachs in Watt et al., 2009 and Alloway et al., 2015). (For interpretation of the references to colour in this figure legend, the reader is referred to the Web version of this article.)

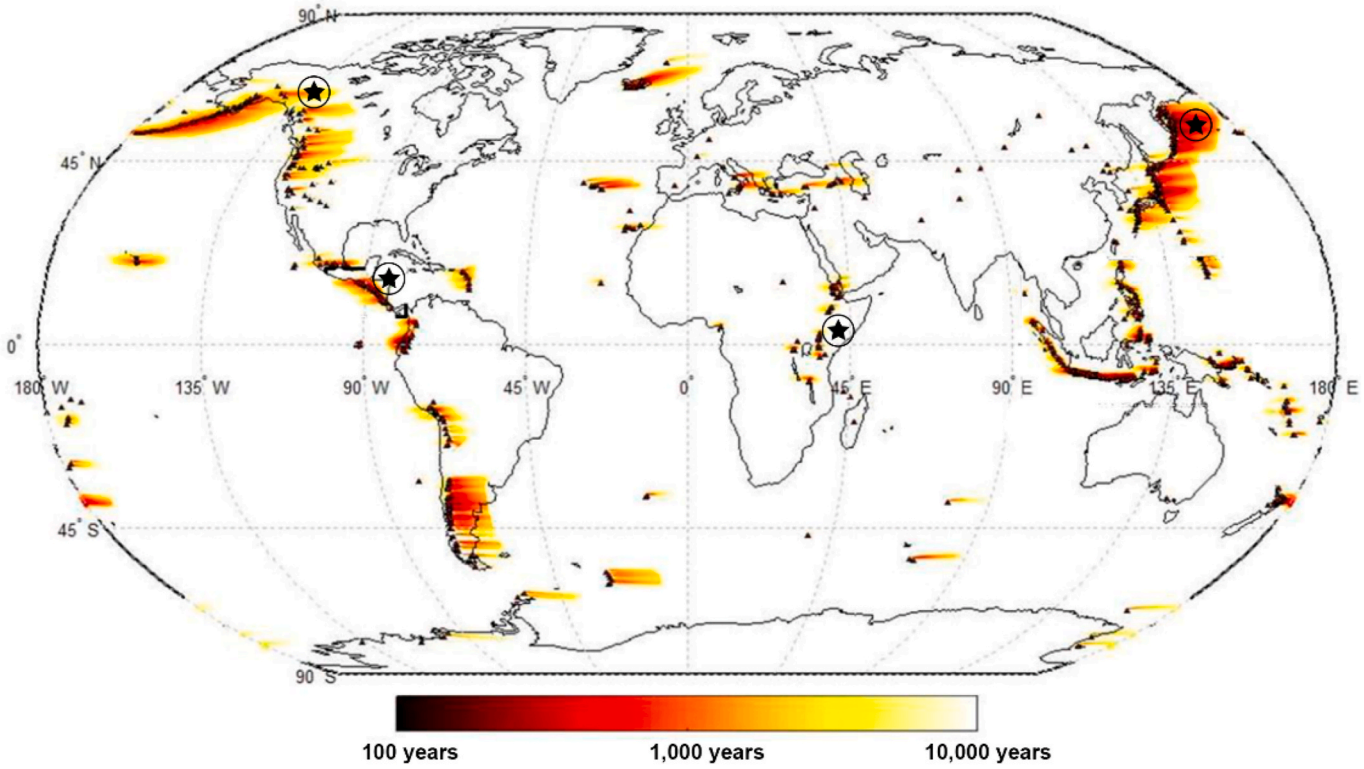

Fig. 7. Global map of probabilistic ash fall hazard (the average recurrence interval in years between ash fall thicknesses exceeding 1 mm) with some important archeological regions located closed to volcanic areas represented by black stars (modified from Jenkins et al., 2015).

complex) deposited ash across the region refreshing the pool of primary volcanic mineral to local soils (Alloway et al., 2015, 2017; Romero et al., 2016).

The isotopic composition of 0.7040–0.7050 registered in Río Negro is related to that of the southern Andean arc. Almost all volcanoes between ~39 and 43°S have a basic to intermediate composition and their tephra have $^{87}Sr/^{86}Sr$ around 0.7040. The only exception is the Chaitén with a rhyolitic composition and tephra with $^{87}Sr/^{86}Sr$ ~0.7050 (Hickey-Vargas et al., 2016). The transition from unradiogenic (~0.7040–0.7050) to more radiogenic ratios (>0.7050) in bioavailable $^{87}Sr/^{86}Sr$ fits with the isopachs from the recent eruptions from Chaitén and Puyehue-Cordón Caulle complex (Fig. 6). As volcanic ashes are deposited following the dominant westerlies, their thickness and their particle size decrease eastward from the volcano (Watt et al., 2009; Jenkins et al., 2015). This pattern also explains why the random forest model selected elevation as a relevant predictor of bioavailable $^{87}Sr/^{86}Sr$. Both ash deposition and volcanic sediment transport decrease eastward from the Andes to the low-lying arid Atlantic plains. The bioavailable $^{87}Sr/^{86}Sr$ is lowest at higher elevation because of the closeness to the volcanic centers where fresh volcaniclastic materials are constantly supplied, and highest on the Atlantic plains where less fresh volcanic material is available to form soils (Fig. 6).

The impact of tephra deposition becomes weaker eastward, but the aeolian cover that dominates northeastern Río Negro -and southern Pampas- is still characterized by a volcaniclastic composition (Zárate and Tripaldi, 2012). The $^{87}Sr/^{86}Sr$ of the samples from Atlantic plains are higher than those expected if Quaternary Andean volcaniclastic sediments were the only source of sediments to those ecosystems. This is because Patagonian sediments (i.e. top soil, bed sediments and aeolian dust) have an important contribution (~40%) of silicic Jurassic volcanic products, that explains the higher ratios in northeastern Río Negro, that differ from the average mantle-derived materials and the younger Andean volcanism (Gaiero et al., 2004, 2007). The ratios of these sediments were achieved during the Pleistocene, during the onset of the southern Andean volcanism ($^{87}Sr/^{86}Sr_{mean} \approx 0.7060$ and $^{87}Sr/^{86}Sr_{range} \approx 0.7040–0.7080$ from ~38°S to 51°40′S -excluding samples from Bahía Blanca-). Both sources of sediments were transported by glacier, water and wind, mixing and forming loess of intermediate isotopic composition (Gaiero et al., 2007; Gili et al., 2017). This reworking of more radiogenic volcaniclastic sediments explains why dust deposition is selected as a key predictor of bioavailable $^{87}Sr/^{86}Sr$. Dust deposition of radiogenic reworked loess is larger in the low-lying and arid regions of northeastern Río Negro explaining the higher but relatively homogenous bioavailable $^{87}Sr/^{86}Sr$ over those locations (Fig. 6).

The most radiogenic ratios of the study area (>0.7070) are clustered in the A-NMP sector, between the Somuncurá Plateau and the coast (Fig. 6). These higher bioavailable $^{87}Sr/^{86}Sr$ could reflect the input of more local eroded material from the elderly geologic formations that outcrops around the eastern margin of the North Patagonian Massif (Fig. 4). As a part of the Jurassic silicic province of Chon Aike, the Marifil Formation is dominated by highly evolved intermediate-felsic rhyolites with $^{87}Sr/^{86}Sr$ spanning from 0.7070 to >0.8000 at Sierra Pailemán and from 0.7100 to >0.8000 at Sierra Grande (Pankhurst and Rapela, 1995; Pankhurst et al., 1998). These rock units are prone to aeolian erosion and could contribute to the local dust sources. Another potential more radiogenic sources that could contribute to the local bioavailable $^{87}Sr/^{86}Sr$ in this region include granites from Sierra Grande and Arroyo Salado ($^{87}Sr/^{86}Sr \approx 0.7200$), metasedimentary rocks from El Jagüelito Formation, Nahuel Niyeu Formation and Mina Gonzalito complex ($^{87}Sr/^{86}Sr > 0.7200$) (Pankhurst et al., 2006; see also granitoid ratios in Varela et al., 2009) or marble and limestone from Sierras de Pailemán ($^{87}Sr/^{86}Sr \approx 0.7070$), Mina Gonzalito ($^{87}Sr/^{86}Sr \approx 0.7080$) and Sierra Grande ($^{87}Sr/^{86}Sr \approx 0.7100$) (Varela et al., 2014).

3.5. Provenance studies in volcanic regions

The central role of volcanic deposition in Río Negro highlights that even hundreds of kilometers away from volcanoes, tephra can still be a

key contributor to the bioavailable $^{87}Sr/^{86}Sr$ and could potentially vary at Quaternary timescales, at least between glacial and interglacial periods. This observation is particularly relevant for archaeology because several key regions around the globe are located near active volcanic centers. For example, studies on early hominids are located close to the East African rift, early dispersal of humans in the Americas involve paths along volcanic arc regions (e.g. Beringia, western North America), or several cultural developments in Mesoamerica and South America are intimately linked to volcanic arc settings (Fig. 7). Research projects in any of these regions involving $^{87}Sr/^{86}Sr$ should consider the Quaternary volcanic history of the region to better understand how the bioavailable $^{87}Sr/^{86}Sr$ might have varied in the past and, therefore, to conceive more accurate archeological expectations and inferences.

Given the importance of Quaternary volcanic processes and atmospheric deposition in Río Negro, one emerging question is whether the isoscape developed in this study is suitable for archeological paleomobility studies. Based on our results and the available information, we consider that this isoscape is useful not only for provenance applications in the present but should also be valid for most of Holocene. First, both volcanic and wind activities have been relatively stable during most of that time in the region. Large tephrochronological sequences and paleoecological reconstructions have shown that Patagonia has been affected by an intense explosive volcanic activity and by westerly winds during the entire Holocene (Stern, 2004; Gaiero et al., 2007; Fontijn et al., 2014, 2016; Brown et al., 2015; Alloway et al., 2017; Gili et al., 2017; among others). Second, most of the loess deposition and volcaniclastic sediment transport took placed during previous glacial periods of the Pleistocene (Gaiero et al., 2007). Considering that soils have been influenced by relatively regular volcanism, and atmospheric deposition from established sources, it is likely that the overall pattern of bioavailable $^{87}Sr/^{86}Sr$ remained relatively constant across Río Negro throughout the Holocene. Third, archeological studies in the region only cover the last 3500 years BP further limiting potential geomorphological variations (Mariano, 2011; Fernández et al., 2013; Prates and Di Prado, 2013; Serna, 2018; Serna and Romano, 2018; Mange, 2019).

4. Conclusions

In this study, we found that bioavailable $^{87}Sr/^{86}Sr$ ratios across Río Negro show little variation and differ from those of the local geological units. The bioavailable $^{87}Sr/^{86}Sr$ also displays a gradual increase eastward inversely correlating to the elevation gradient and positively correlating with the rate of dust deposition. We argue that this pattern reflects the interaction of two main atmospheric sources of Sr to local ecosystems: 1) fresh unradiogenic Andean volcanic tephra and 2) reworked loess mixing Quaternary and Jurassic volcaniclastic sediments. Higher deposition rates of fresh unradiogenic tephra occur close to the Andes explaining the lower $^{87}Sr/^{86}Sr$ in this region. Even if the tephra deposition rate is low, the bioavailable $^{87}Sr/^{86}Sr$ remains low and unrelated to the local geology. The availability of fresh unradiogenic mineral decreases eastward away from the main volcanic centers. In these low-lying and arid regions, atmospheric deposition of reworked volcaniclastic glacial loess transported from the Andes by glaciers, rivers and wind, is the dominant source of Sr to ecosystems. While bioavailable $^{87}Sr/^{86}Sr$ pattern certainly varied during glacial/interglacial periods in Río Negro, it might have remained stable throughout the Holocene.

This case study demonstrates that, in volcanic areas, bioavailable $^{87}Sr/^{86}Sr$ data should be carefully interpreted for archeological studies across the Quaternary. In these volcanic regions, highly erodible and weatherable volcanic material can lead to bioavailable $^{87}Sr/^{86}Sr$ variation across large spatial scales and at archeologically-relevant timescales. This finding is particularly relevant since several archeological regions around the world are close to volcanic centers. Having a good understanding of Quaternary geomorphological processes is therefore key to properly interpret $^{87}Sr/^{86}Sr$ data in paleomobility studies.

Acknowledgments

We acknowledge the SPATIAL (Spatio-temporal Isotope Analytics Lab, University of Utah) Short Course and the NSF award #1137336 Inter-university Training in Continental-scale Ecology (United States) for providing the environment to design this work and the funds to carry it out to A.S. Also to the support from PIP-CONICET-0244 and PICT2015-3645 (Argentina) to L.P., DCSG's UCT Fund (427277) (South Africa) and NSERC Discovery Grant RGPIN-2019-05709 (Canada) to C. P.B. To P.J. le Roux, F. Rawoot and K. Grey for technical assistance. Special thanks to Juan Prates for his invaluable help during the sampling field trip. To S.F.L. Watt, B.V. Alloway and P.I. Moreno for kindly share the isopachs from Fig. 5, and S. Jenkins and T. Wilson for their permission to reuse and modify Fig. 6. We also thank the Editor and the two anonymous reviewers for their useful comments, who helped to improve the clarity and quality of the manuscript.

Appendix A. Supplementary data

Supplementary data to this article can be found online at https://doi.org/10.1016/j.jas.2020.105198.

References

Alloway, B.V., Pearce, N.J., Moreno, P.I., Villarosa, G., Jara, I., De Pol-Holz, R., Outes, V., 2017. An 18,000 year-long eruptive record from Volcán Chaitén, northwestern Patagonia: paleoenvironmental and hazard-assessment implications. Quat. Sci. Rev. 168, 151–181. https://doi.org/10.1016/j.quascirev.2017.05.011.

Alloway, B.V., Pearce, N.J., Villarosa, G., Outes, V., Moreno, P.I., 2015. Multiple melt bodies fed the AD 2011 eruption of Puyehue-Cordón Caulle, Chile. Sci. Rep. 5, 17589. https://doi.org/10.1038/srep17589.

Amigo, Á., Lara, L.E., Smith, V.C., 2013. Holocene record of large explosive eruptions from Chaitén and Michinmahuida Volcanoes, Chile. Andean Geol. 40 (2), 227–248. https://doi.org/10.5027/andgeoV40n2-a03.

Barberena, R., Durán, V.A., Novellino, P., Winocur, D., Benítez, A., Tessone, A., Quiroga, M.N., Marsh, E.J., Gasco, A., Cortegoso, V., Lucero, G., Llano, C., Knudson, K.J., 2017. Scale of human mobility in the southern Andes (Argentina and Chile): a new framework based on strontium isotopes. Am. J. Phys. Anthropol. 164 (2), 305–320. https://doi.org/10.1002/ajpa.23270.

Barberena, R., Tessone, A., Cagnoni, M., Gasco, A., Durán, V., Winocur, D., Benítez, A., Lucero, G., Trillas, D., Zonana, I., Novellino, P., Fernández, M., Bavio, M.A., Zubillaga, E., Gautier, E.A., 2019. Bioavailable strontium in the southern Andes (Argentina and Chile): a tool for tracking human and animal movement. Environ. Archaeol. 1–13 https://doi.org/10.1080/14614103.2019.1689894.

Basei, M.A., Varela, R., Passarelli, C., Siga Jr., O., Cingolani, C., Sato, A., Gonzalez, P.D., 2005. The crystalline basement in the north of Patagonia: isotopic ages and regional characteristics. Gondwana 12, 62.

Bataille, C.P., Bowen, G.J., 2012. Mapping 87Sr/86Sr variations in bedrock and water for large scale provenance studies. Chem. Geol. 304, 39–52. https://doi.org/10.1016/j.chemgeo.2012.01.028.

Bataille, C.P., Brennan, S.R., Hartmann, J., Moosdorf, N., Wooller, M.J., Bowen, G.J., 2014. A geostatistical framework for predicting variations in strontium concentrations and isotope ratios in Alaskan rivers. Chem. Geol. 389, 1–15. https://doi.org/10.1016/j.chemgeo.2014.08.030.

Bataille, C.P., Laffoon, J., Bowen, G.J., 2012. Mapping multiple source effects on the strontium isotopic signatures of ecosystems from the circum-Caribbean region. Ecosphere 3 (12), 1–24. https://doi.org/10.1890/ES12-00155.1.

Bataille, C.P., von Holstein, I.C., Laffoon, J.E., Willmes, M., Liu, X.M., Davies, G.R., 2018. A bioavailable strontium isoscape for Western Europe: a machine learning approach. PloS One 13 (5), e0197386. https://doi.org/10.1371/journal.pone.0197386.

Beard, B.L., Johnson, C.M., 2000. Strontium isotope composition of skeletal material can determine the birth place and geographic mobility of humans and animals. J. Forensic Sci. 45 (5), 1049–1061.

Bentley, R.A., 2006. Strontium isotopes from the earth to the archaeological skeleton: a review. J. Archaeol. Method Theor 13 (3), 135–187. https://doi.org/10.1007/s10816-006-9009-x.

Blasi, A., Manassero, M.J., 1990. The Colorado River of Argentina: source, climate, and transport as controlling factors on sand composition. J. South Am. Earth Sci. 3 (1), 65–70. https://doi.org/10.1016/0895-9811(90)90018-V.

Blisniuk, P.M., Stern, L.A., Chamberlain, C.P., Idleman, B., Zeitler, P.K., 2005. Climatic and ecologic changes during miocene surface uplift in the southern patagonian Andes. Earth Planet Sci. Lett. 230 (30), 125–142.

Brown, S.K., Sparks, R.S.J., Mee, K., Vye-Brown, C., Ilyinskaya, E., Jenkins, S.F., Loughlin, S.C., 2015. Country and regional profiles of volcanic hazard and risk: appendix B – region 15. In: Loughlin, S.C., Sparks, R.S.J., Brown, S.K., Jenkins, S.F., Vye-Brown, C. (Eds.), Global Volcanic Hazards and Risk. Cambridge University Press, Cambridge, pp. 599–663.

Capo, R.C., Stewart, B.W., Chadwick, O.A., 1998. Strontium isotopes as tracers of ecosystem processes: theory and methods. Geoderma 82 (1–3), 197–225.

Coronato, A., Martínez, O., Rabassa, J., 2004. Glaciations in Argentine Patagonia, southern South America. In: Ehlers, J., Gibbard, P.L. (Eds.), Quaternary Glactations-Extent and Chronology, Part III. Elsevier, Amsterdam, pp. 49–67.
Crowley, B.E., Miller, J.H., Bataille, C.P., 2017. Strontium isotopes (87Sr/86Sr) in terrestrial ecological and palaeoecological research: empirical efforts and recent advances in continental-scale models. Biol. Rev. 92 (1), 43–59. https://doi.org/10.1111/brv.12217.
Cucchi, R., Busteros, A., Lema, H., 2001. Hoja geológica 4169 II, los Menucos, provincia de Río Negro. Instituto de Geología y Recursos Minerales SEGEMAR, Boletín 265, 1–105.
Dalla Salda, L.H., Varela, R., Cingolani, C., Aragón, E., 1994. The rio chico paleozoic crystalline complex and the evolution of northern Patagonia. J. South Am. Earth Sci. 7 (3–4), 377–386.
Escosteguy, L., Etcheverría, M.P., Folguera, A., Franchi, M., Faroux, A., Getin, P., 2011. Hoja geológica 3966- IV, choele choel. Provincia de Río Negro. Instituto de Geología y Recursos Minerales SEGEMAR, Boletín 398, 38.
Evans, J.A., Montgomery, J., Wildman, G., Boulton, N., 2010. Spatial variations in biosphere 87Sr/86Sr in Britain. J. Geol. Soc. 167 (1), 1–4.
Fenner, J.N., Wright, L.E., 2014. Revisiting the strontium contribution of sea salt in the human diet. J. Archaeol. Sci. 44, 99–103. https://doi.org/10.1016/j.jas.2014.01.020.
Fernández, P.M., Carballido Calatayud, M., Bellelli, C., Podestá, M., 2013. Tiempo de cazadores. Cronología de las ocupaciones humanas en el valle del río Manso inferior (Río Negro). In: Zangrando, A., Barberena, R., Gil, A., Neme, G., Giardina, M., Luna, L., Otaola, C., Paulides, S., Salgán, L., Tivoli, A. (Eds.), Tendencias teórico-metodológicas y casos de estudio en la arqueología de Patagonia. Museo de Historia Natural de San Rafael, SAA e INAPL, Buenos Aires, pp. 167–175.
Fidalgo, F., Rabassa, J., 1984. Los depósitos cuaternarios. In: Ramos, V. (Ed.), Geología y Recursos Naturales de la Provincia de Río Negro: Relatorio del IX Congreso Geológico Argentino. Servicio Geológico Nacional, Buenos Aires, pp. 301–316.
Flockhart, D.T., Kyser, T.K., Chipley, D., Miller, N.G., Norris, D.R., 2015. Experimental evidence shows no fractionation of strontium isotopes (87Sr/86Sr) among soil, plants, and herbivores: implications for tracking wildlife and forensic science. Isot. Environ. Health Stud. 51 (3), 372–381.
Folguera, A., Zárate, M., 2009. La sedimentación neógena continental en el sector extrandino de Argentina central. Rev. Asoc. Geol. Arg. 64 (4), 692–712.
Fontijn, K., Lachowycz, S.M., Rawson, H., Pyle, D.M., Mather, T.A., Naranjo, J.A., Moreno-Roa, H., 2014. Late Quaternary tephrostratigraphy of southern Chile and Argentina. Quat. Sci. Rev. 89, 70–84. https://doi.org/10.1016/j.quascirev.2014.02.007.
Fontijn, K., Rawson, H., Van Daele, M., Moernaut, J., Abarzúa, A.M., Heirman, K., Bertrand, S., Pyle, D.M., Mather, T.A., De Batist, M., Naranjo, J.A., Moreno, H., 2016. Synchronisation of sedimentary records using tephra: a postglacial tephrochronological model for the Chilean Lake District. Quat. Sci. Rev. 137, 234–254. https://doi.org/10.1016/j.quascirev.2016.02.015.
Franchi, M.R., Nullo, F., Sepúlveda, E., Uliana, A., 1984. Las sedimentitas terciarias. In: Ramos, V. (Ed.), Geología y Recursos Naturales de la Provincia de Río Negro: Relatorio del IX Congreso Geológico Argentino. Servicio Geológico Nacional, Buenos Aires, pp. 215–266.
Frei, K.M., 2013. Exploring the potential of the strontium isotope tracing system in Denmark. Dan. J. Archaeol. 1 (2), 113–122. https://doi.org/10.1080/21662282.2012.760889.
Frei, K.M., Frei, R., 2011. The geographic distribution of strontium isotopes in Danish surface waters – a base for provenance studies in archaeology, hydrology and agriculture. Appl. Geochem. 26, 326–340. https://doi.org/10.1016/j.apgeochem.2010.12.006.
Gaiero, D.M., 2007. Dust provenance in Antarctic ice during glacial periods: from where in southern South America? Geophys. Res. Lett. 34 (17).
Gaiero, D.M., Brunet, F., Probst, J.L., Depetris, P.J., 2007. A uniform isotopic and chemical signature of dust exported from Patagonia: rock sources and occurrence in southern environments. Chem. Geol. 238 (1–2), 107–120.
Gaiero, D.M., Depetris, P.J., Probst, J.L., Bidart, S.M., Leleyter, L., 2004. The signature of river-and wind-borne materials exported from Patagonia to the southern latitudes: a view from REEs and implications for paleoclimatic interpretations. Earth Planet Sci. Lett. 219 (3–4), 357–376.
Gaiero, D.M., Probst, J.L., Depetris, P.J., Bidart, S.M., Leleyter, L., 2003. Iron and other transition metals in Patagonian riverborne and windborne materials: geochemical control and transport to the southern South Atlantic Ocean. Geochem. Cosmochim. Acta 67 (19), 3603–3623.
Gaiero, D.M., Probst, J.L., Depetris, P.J., Leleyter, L., Kempe, S., 2002. Riverine transfer of heavy metals from Patagonia to the southwesten Atlantic Ocean. Reg. Environ. Change 3, 51–64.
Gaitán, J., Ayesa, J., Umaña, F., Raffo, F., Bran, D., 2011. Cartografía del área afectada por cenizas volcánicas en las provincias de Río Negro y Neuquén. Instituto Nacional de Tecnología Agropecuaria (INTA), San Carlos de Bariloche.
Genuer, R., Poggi, J.M., Tuleau-Malot, C., 2015. VSURF: an R package for variable selection using random forests. R J 7, 19–33.
Gili, S., Gaiero, D.M., Goldstein, S.L., Chemale Jr., F., Jweda, J., Kaplan, M.R., Becchio, R., Koester, E., 2017. Glacial/interglacial changes of Southern Hemisphere wind circulation from the geochemistry of South American dust. Earth Planet Sci. Lett. 469, 98–109.
Godagnone, E.R., Cuenca, M.A., et al., 2010. Estudio de Suelos del Área Sur. INTA, Buenos Aires.
González Díaz, E.F., Malagnino, E.C., 1984. Geomorfología de la provincia de Río Negro. In: Ramos, V. (Ed.), Geología y Recursos Naturales de la Provincia de Río Negro: Relatorio del IX Congreso Geológico Argentino. Servicio Geológico Nacional, Buenos Aires, pp. 347–364.
Graustein, W.C., 1989. 87 Sr/86 Sr ratios measure the sources and flow of strontium in terrestrial ecosystems. In: Rundel, P.W., Ehleringer, J.R., Nagy, K.A. (Eds.), Stable Isotopes in Ecological Research. Ecological Studies (Analysis and Synthesis), vol. 68. Springer, New York, pp. 491–512.
Hajj, F., Poszwa, A., Bouchez, J., Guérold, F., 2017. Radiogenic and "stable" strontium isotopes in provenance studies: a review and first results on archaeological wood from shipwrecks. J. Archaeol. Sci. 86, 24–49. https://doi.org/10.1016/j.jas.2017.09.005.
Hartmann, J., Moosdorf, N., 2012. The new global lithological map database GLiM: a representation of rock properties at the Earth surface. Geochem. Geophys. Geosyst. 13 https://doi.org/10.1029/2012GC004370.
Hartman, G., Richards, M., 2014. Mapping and defining sources of variability in bioavailable strontium isotope ratios in the Eastern Mediterranean. Geochem. Cosmochim. Acta 126, 250–264. https://doi.org/10.1016/j.gca.2013.11.015.
Haverkort, C.M., Weber, A., Katzenberg, M.A., Goriunova, O.I., Simonetti, A., Creaser, R., 2008. Hunter-gatherer mobility strategies and resource use based on strontium isotope (87Sr/86Sr) analysis: a case study from Middle Holocene Lake Baikal, Siberia. J. Archaeol. Sci. 35 (5), 1265–1280.
Hengl, T., Mendes de Jesus, J., Heuvelink, G.B.M., Ruiperez Gonzalez, M., Kilibarda, M., Blagotić, A., et al., 2017. SoilGrids250m: global gridded soil information based on machine learning. PloS One 12, e0169748. https://doi.org/10.1371/journal.pone.0169748.
Hickey-Vargas, R., Holbik, S., Tormey, D., Frey, F., Roa, H., 2016. Basaltic rocks from the Andean Southern Volcanic Zone: insights from the comparison of along-strike and small-scale geochemical variations and their sources. Lithos 258, 115–132.
Hijmans, R.J., Cameron, S.E., Parra, J.L., Jones, P.G., Jarvis, A., 2005. Very high resolution interpolated climate surfaces for global land areas. Int. J. Climatol. 25, 1965–1978. https://doi.org/10.1002/joc.1276.
Hodell, D.A., Quinn, R.L., Brenner, M., Kamenov, G., 2004. Spatial variation of strontium isotopes (87Sr/86Sr) in the Maya region: a tool for tracking ancient human migration. J. Archaeol. Sci. 31 (5), 585–601.
Hugo, C., Leanza, H.A., 2001. Hoja Geológica 3969-IV. General Roca, provincias del Neuquén y Río Negro. Instituto de Geología y Recursos Naturales, SEGEMAR, Boletín 308, 1–71.
Iriondo, M., 2000. Patagonian dust in Antarctica. Quat. Int. 68, 83–86.
Jarvis, A., Reuter, A., Nelson, A., Guevara, E., 2008. Hole-filled SRTM for the Globe Version 4, Available from the CGIAR-CSI SRTM 90m Database. CGIAR CSI Consort Spat Inf., pp. 1–9. http://srtm.csi.cgiar.org
Jenkins, S.F., Wilson, T.M., Magill, C.R., Miller, V., Stewart, C., Marzocchi, W., Boulton, M., 2015. Volcanic Ash Fall Hazard and Risk: Technical Background Paper for the UNISDR 2015 Global Assessment Report on Disaster Risk Reduction. Global Volcano Model and IAVCEI.
Kootker, L.M., van Lanen, R., Kars, H., Davies, G., 2016. Strontium isoscapes in The Netherlands. Spatial variations in 87Sr/86Sr as a proxy for palaeomobility. J. Archaeol. Sci. Rep. 6, 1–13.
Kuhn, M., 2008. Building predictive models in R using the caret package. J. Stat. Software 28, 1–26.
Lengfelder, F., Grupe, G., Stallauer, A., Huth, R., Söllner, F., 2019. Modelling strontium isotopes in past biospheres–Assessment of bioavailable 87Sr/86Sr ratios in local archaeological vertebrates based on environmental signatures. Sci. Total Environ. 648, 236–252.
Lewis, J., Pike, A., Coath, C., Evershed, R., 2017. Strontium concentration, radiogenic (87Sr/86Sr) and stable (δ 88Sr) strontium isotope systematics in a controlled feeding study. Star: Sci. Technol. Archaeol. Res. 3 (1), 45–57.
Luchsinger, H.M., 2006. The Late Quaternary Landscape History of the Middle Río Negro Valley, Northern Patagonia, Argentina: its Impact on Preservation of the Archaeological Record and Influence on Late Holocene Human Settlement Patterns. Unpublished Ph.D. Thesis, Texas A&M University, USA.
Mahowald, N.M., Muhs, D.R., Levis, S., Rasch, P.J., Yoshioka, M., Zender, C.S., et al., 2006. Change in atmospheric mineral aerosols in response to climate: last glacial period, preindustrial, modern, and doubled carbon dioxide climates. J. Geophys. Res. Atmos. 111 https://doi.org/10.1029/2005JD006653.
Mange, E., 2019. Investigaciones arqueológicas en la margen sur del valle medio-superior del río Negro (Pcia de Río Negro). Unpublished Ph.D. Thesis, University of La Plata, Argentina.
Mariano, C., 2011. Prácticas mortuorias y registro bioarqueológico en la costa rionegrina del golfo San Matías, Argentina. Intersecc. Antropol. 12, 17–30.
Martínez, O., Rabassa, J., 2014. The rhyolitic plateau of the Marifil Formation (jurassic): a gondwana paleosurface in the southeastern portion of the northern Patagonia Massif. In: Rabassa, J., Ollier, C. (Eds.), Gondwana Landscapes in Southern South America. Springer, Dordrecht, pp. 447–476.
Martínez, O., Rabassa, J., Coronato, A., 2009. Charles Darwin and the first scientific observations on the Patagonian shingle formation (Rodados Patagónicos). Rev. Asoc. Geol. Arg. 64 (1), 90–100.
Montgomery, J., 2010. Passports from the past: investigating human dispersals using strontium isotope analysis of tooth enamel. Ann. Hum. Biol. 37 (3), 325–346.
Mooney, W.D., Laske, G., Masters, T.G., 1998. Crust 5.1: a global crustal model at 5° × 5°. J. Geophys. Res. Solid Earth 103, 727–747. https://doi.org/10.1029/97JB02122.
Nafplioti, A., 2011. Tracing population mobility in the Aegean using isotope geochemistry: a first map of local biologically available 87Sr/86Sr signatures. J. Archaeol. Sci. 38 (7), 1560–1570.

Panebianco, J., Mendez, M., Buschiazzo, D., Bran, D., Gaitán, J., 2017. Dynamics of volcanic ash remobilisation by wind through the Patagonian steppe after the eruption of Cordón Caulle, 2011. Sci. Rep. 7, 45529.
Pankhurst, R., Leat, P., Sruoga, P., Rapela, C., Márquez, M., Storey, B., Riley, T., 1998. The Chon Aike province of Patagonia and related rocks in West Antarctica: a silicic large igneous province. J. Volcanol. Geoth. Res. 81 (1–2), 113–136.
Pankhurst, R., Rapela, C., 1995. Production of Jurassic rhyolite by anatexis of the lower crust of Patagonia. Earth Planet Sci. Lett. 134 (1–2), 23–36.
Pankhurst, R., Rapela, C., Fanning, C., Márquez, M., 2006. Gondwanide continental collision and the origin of Patagonia. Earth Sci. Rev. 76 (3–4), 235–257.
Paruelo, J., Beltrán, A., Jobbágy, E., Sala, O., Golluscio, R., 1998. The climate of Patagonia: general patterns and controls on biotic processes. Asociación Argentina de Ecología. Ecol. Austral 8, 85–101.
Prates, L., 2008. Los indígenas del Río Negro. Un enfoque arqueológico. Sociedad Argentina de Antropología, Buenos Aires.
Prates, L., Di Prado, V., 2013. Sitios con entierros humanos y ocupaciones residenciales en la cuenca del río Negro (Norpatagonia, Argentina): diacronía y multicausalidad. Lat. Am. Antiq. 24 (4), 451–466.
Prates, L., Mange, E., 2016. Paisajes de tránsito en las planicies y bajos del centro-este de Norpatagonia. Relaciones de la Sociedad Argentina de Antropología 41 (1), 217–236.
Prospero, J., Ginoux, P., Torres, O., Nicholson, S., Gill, T., 2002. Environmental characterization of global sources of atmospheric soil dust identified with the Nimbus 7 Total Ozone Mapping Spectrometer (TOMS) absorbing aerosol product. Rev. Geophys. 40 (1), 2-1.
Ramos, V., 1984. Síntesis. In: Ramos, V. (Ed.), Geología y Recursos Naturales de la Provincia de Río Negro: Relatorio del IX Congreso Geológico Argentino. Servicio Geológico Nacional, Buenos Aires, pp. 3–16.
Rodríguez, M.V., Bertiller, M.B., Bisigato, A., 2007. Are fine roots of both shrubs and perennial grasses able to occupy the upper soil layer? A case study in the arid Patagonian Monte with non-seasonal precipitation. Plant Soil 300 (1–2), 281–288.
Romero, J., Morgavi, D., Arzilli, F., Daga, R., Caselli, A., Reckziegel, F., Viramonte, J., Díaz-Alvarado, J., Polacci, M., Burton, M., Perugini, D., 2016. Eruption dynamics of the 22–23 april 2015 Calbuco volcano (southern Chile): analyses of tephra fall deposits. J. Volcanol. Geoth. Res. 317, 15–29. https://doi.org/10.1016/j.jvolgeores.2016.02.027.
Ryan, S., Snoeck, C., Crowley, Q., Babechuk, M., 2018. 87Sr/86Sr and trace element mapping of geosphere-hydrosphere-biosphere interactions: a case study in Ireland. Appl. Geochem. 92, 209–224. https://doi.org/10.1016/j.apgeochem.2018.01.007.
Schäbitz, F., 2003. Estudios polínicos del Cuaternario en las regiones áridas del sur de Argentina. Revista del Museo Argentino de Ciencias Naturales 5 (2), 291–299.
Serna, A., 2018. Interacciones sociales en el noreste de Patagonia durante el Holoceno tardío: un enfoque bioarqueológico. Unpublished Ph.D. Thesis, University of La Plata, Argentina.
Serna, A., Romano, V., 2018. Rescates bioarqueológicos en el valle medio del río Negro (provincia de Río Negro): el potential informativo del registro altamente perturbado. Revista Argentina de Antropología Biológica 20 (2), 1–12.
Serna, A., Prates, L., Flensborg, G., Martínez, G., Favier Dubois, C., Perez, S.I., 2019a. Does the shape make a difference? Evaluating the ethnic role of cranial modification in the Pampa-Patagonia region (Argentina) during the late Holocene. Archaeol. Anthropol. Sci. 11 (6), 2597–2610. https://doi.org/10.1007/s12520-018-0687-6.
Serna, A., Prates, L., Valenzuela, L.O., Salazar-García, D.C., 2019b. Back to the bases: building a terrestrial water δ18O baseline for archaeological studies in North Patagonia (Argentina). Quat. Int. https://doi.org/10.1016/j.quaint.2019.06.008.
Snoeck, C., Pouncett, J., Claeys, P., Goderis, S., Mattielli, N., Pearson, M.P., Willis, C., Zazzo, A., Lee-Thorp, J., Schulting, R., 2018. Strontium isotope analysis on cremated human remains from Stonehenge support links with west Wales. Sci. Rep. 8 (1), 10790. https://doi.org/10.1038/s41598-018-28969-8.
Soldano, F.A., 1947. Régimen y aprovechamiento de la red flvial argentina. Parte 1. El Río Paraná Y sus Tributarios. Editorial Cimera, Buenos Aires.
Spalletti, L., Isla, F., 2003. Características y evolución del delta del río Colorado ("Colú-Leuvú"), provincia de Buenos Aires, República Argentina. Rev. Asoc. Arg. Sedimentol. 10 (1), 23–37.
Stern, C., 2004. Active Andean volcanism: its geologic and tectonic setting. Rev. Geol. Chile 31 (2), 161–206.
Varela, R., Basei, M., Cingolani, C., Siga Jr., O., Passarelli, C., 2005. El Basamento Cristalino de los Andes norpatagónicos en Argentina: geocronología e interpretación tectónica. Rev. Geol. Chile 32, 167–182.
Varela, R., González, P., Philipp, R., Sato, A., González, S., Greco, G., Naipauer, M., 2014. Isótopos de estroncio en calcáreos del noreste Patagónico: resultados preliminares. Rev. Asoc. Geol. Arg. 71 (4), 526–536.
Varela, R., Sato, K., González, P., Sato, A., Basei, M., 2009. Geología y geocronología Rb-Sr de granitoides de Sierra Grande, provincia de Río Negro. Rev. Asoc. Geol. Arg. 64 (2), 275–284.
Villalba-Mouco, V., Sauqué, V., Sarasketa-Gartzia, I., Pastor, M., le Roux, P., Vicente, D., Utrilla, P., Salazar-García, D.C., 2018. Territorial mobility and subsistence strategies during the ebro basin late neolithic-chalcolithic: a multi-isotope approach from san juan cave (loarre, Spain). Quat. Int. 481, 28–41. https://doi.org/10.1016/j.quaint.2017.05.051.
Villarosa, G., Outes, V., Hajduk, A., Montero, E., Sellés, D., Fernández, M., Crivelli, E., 2006. Explosive volcanism during the Holocene in the upper limay river basin: the effects of ashfalls on human societies, northern Patagonia, Argentina. Quat. Int. 158 (1), 44–57.
Watt, S.F., Pyle, D.M., Mather, T.A., 2013. Evidence of mid-to late-Holocene explosive rhyolitic eruptions from Chaitén Volcano, Chile. Andean Geol. 40 (2), 216–226. https://doi.org/10.5027/andgeoV40n2-a02.
Watt, S.F., Pyle, D.M., Mather, T.A., Martin, R.S., Matthews, N.E., 2009. Fallout and distribution of volcanic ash over Argentina following the May 2008 explosive eruption of Chaitén, Chile. J. Geophys. Res.: Solid Earth 114 (B4). https://doi.org/10.1029/2008JB006219.
Willmes, M., Bataille, C.P., James, H., Moffat, I., McMorrow, L., Kinsley, L., Armstrong, R.A., Eggins, S., Grün, R., 2018. Mapping of bioavailable strontium isotope ratios in France for archaeological provenance studies. Appl. Geochem. 90, 75–86. https://doi.org/10.1016/j.apgeochem.2017.12.025.
Willmes, M., Mcmorrow, L., Kinsley, L., Armstrong, R.A., Aubert, M., Eggins, S., Falguères, C., Maureille, B., Moffat, I., Grün, R., 2014. The IRHUM (Isotopic Reconstruction of Human Migration) database-bioavailable strontium isotope ratios for geochemical fingerprinting in France. Earth Syst. Sci. Data 6, 117–122. https://doi.org/10.5194/essdd-6-761-2013.
Zar, J.H., 1999. Biostatistical Analysis. Pearson Education India, Delhi.
Zárate, M., 2003. Loess of southern south America. Quat. Sci. Rev. 22 (18–19), 1987–2006. https://doi.org/10.1016/S0277-3791(03)00165-3.
Zárate, M., Blasi, A., 1993. Late Pleistocene-Holocene eolian deposits of the southern Buenos Aires Province, Argentina: a preliminary model. Quat. Int. 17, 15–20. https://doi.org/10.1016/1040-6182(93)90075-Q.
Zárate, M., Tripaldi, A., 2012. The aeolian system of central Argentina. Aeolian Res 3 (4), 401–417. https://doi.org/10.1016/j.aeolia.2011.08.002.